JAIST Repository
https://dspace.jaist.ac.jp/

Title	Improving crystalline quality of polycrystalline silicon thin films crystallized on yttria-stabilized zirconia crystallization-induction layers by the two-step irradiation method of pulsed laser annealing
Author(s)	Mai, Thi Kieu Lien; Horita, Susumu
Citation	Japanese Journal of Applied Physics, 54(3S): 03CA01-1-03CA01-8
Issue Date	2015-02-18
Type	Journal Article
Text version	author
URL	http://hdl.handle.net/10119/12612
Rights	This is the author's version of the work. It is posted here by permission of The Japan Society of Applied Physics. Copyright (C) 2015 The Japan Society of Applied Physics. Mai Thi Kieu Lien and Susumu Horita, Japanese Journal of Applied Physics, 54(3S), 2015, 03CA01-1-03CA01-8. http://dx.doi.org/10.7567/JJAP.54.03CA01
Description	

JAPAN ADVANCED INSTITUTE OF SCIENCE AND TECHNOLOGY

Japan Advanced Institute of Science and Technology

Improving Crystalline Quality of Poly-Si Thin Films Crystallized on Yttria-Stabilized Zirconia Crystallization-Induction Layers by the Two-Step Irradiation Method of Pulse Laser Annealing

Mai Thi Kieu Lien and Susumu Horita

School of Materials Science, Japan Advanced Institute of Science and Technology, Nomi, Ishikawa 923 – 1292, Japan

E-mail: Mai Thi Kieu Lien (mai.lien@jaist.ac.jp); Susumu Horita (horita@jaist.ac.jp)

Abstract

Crystalline quality of pulse-laser annealed micocrystalline silicon (poly-Si) films on yttria-stabilized zirconia [$(ZrO_2)_{1-x}(Y_2O_3)_x$: YSZ] crystallization-induction (CI) layers is further improved by a new two-step irradiation method, in which amorphous silicon (a-Si) films are irradiated using two kinds of energy density. Firstly, they were irradiated at a low energy density for a short time to generate nuclei, following by irradiation at a high energy density to complete crystallization. Crystalline fraction and grain size of the Si film crystallized by the two-step method were found to be larger while its FWHM was smaller than those by the conventional one. Moreover, grain size of the Si/YSZ/glass was more uniform than that of the Si/glass. This indicates not only effectiveness of the YSZ CI layer but also usefulness of the two-step method on improving Si film quality.

1. Introduction

As semiconductor materials for active channel layer in thin-film transistor (TFT), oxide,[1-3] organic,[4,5] and silicon[6,7] have been studied extensively. However, oxide and organic materials still have some limitations for application in active-matrix flat panel displays (AM-FPDs) such as device instability under bias stress and illumination[8-10] for oxide, and unreliability[11,12] for organic. On the other hand, the most prolonged and widely used channel materials are hydrogenated-amorphous silicon (a-S:H) and polycrystalline silicon (poly-Si). A strong merit of a-Si:H TFT is that it has a lower fabrication cost than that of poly-Si TFT. However, the former has some drawbacks of low carrier mobility (~ $1 cm^2/V.s$), instability, and low reliability,[13-15] which can be addressed by the latter.

Although poly-Si film can be synthesized by a direct deposition method from gas phase,[16-18] a preferred fabrication method is crystallization of amorphous precursor, which can produce higher mobility due to larger grain size and lower crystalline defect density. The crystallization of deposited a-Si films can be carried out by several methods, for instance, solid phase crystallization (SPC),[19-23] metal-induced crystallization (MIC),[24-27] metal-induced lateral crystallization (MILC),[28-31] and pulse laser annealing (PLA).[32-35] Among them, PLA has become a leading technique to fabricate poly-Si films at low temperature because its melting-crystallized films have large grains with high mobility. However, the fabricated poly-Si films by this method have high surface roughness and non-uniform in grain size, which limits the extent of application such as large size FPDs.

Therefore, in order to obtain a poly-Si film with smooth surface and uniform in grain size, we proposed using a crystallization-induction (CI) layer of yttria-stabilized zirconia [$(ZrO_2)_{1-x}(Y_2O_3)_x$: YSZ][36,37] combined with PLA for micro-crystallization with non-

intentional melting.[38,39] It was found that, for an Si/YSZ/glass, interface nucleation is stimulated on the YSZ interface. This is owing to YSZ properties−which are small lattice mismatch and the same cubic crystal structure with Si. On the other hand, for an Si/glass, random Si nucleation occurs on the glass interface due to no crystallographic information of glass. Probably because of this, the grain size of poly-Si film on YSZ layer is more uniform than that on glass.[39] However, before the crystallization growth front from the interface reaches the a-Si film surface, film bulk nucleation occurs even using the YSZ layer, and then crystallization extends around from the nuclei as shown in Fig. 1(a). So, the crystalline quality of a whole Si film becomes poorer.

To further improve the crystalline quality of Si films, we have proposed a new two-step irradiation method (hereafter, two-step method),[40] in which an a-Si film is irradiated using two kinds of irradiation energy densities E as shown in Fig. 1(b). At first, in the initial stage, it is irradiated at a low irradiation energy density E_i for a short time to promote Si nucleation on the YSZ interface with perfect suppression of bulk nucleation. Next, in the second step of growth stage, the Si film is irradiated at a higher irradiation energy density E_g to accelerate the growth from the nuclei and complete the crystallization. The detailed procedure is mentioned later. In fact, the concept of the two-step method is based on the two important findings in the conventional method with a fixed E. The one is the initial nucleation location and the other one is the saturation behavior of crystalline fraction X_c between amorphous and crystalline Si with respect to pulse number. Regarding the X_c saturation behavior, as shown in the previous paper,[39] the X_c increases with the pulse number N and has saturation tendency around some number, e.g., 10, at a fixed E and the saturation values increases with increasing E.

In this paper, we at first show the clear observation results on Si nucleation location by Raman spectroscopy and explain the reason why X_c saturation behavior is important concept for the two-step method. Then, we report the detailed investigation results on quality of crystallized Si films with/without the YSZ layers by the two-step method in PLA, comparing with the conventional method. Crystalline quality of the crystallized Si films was estimated mainly by the two kinds of Raman spectroscopies, which are measured by a helium-neon (He-Ne) laser beam and a helium-cadmium (He-Cd) laser beam, individually. The former is used for average estimation of a whole film while the latter is used for local estimation near the interface and surface of the crystallized Si films.

2. Experimental

A 60-nm YSZ CI layer with a preferential orientation of (111)[39] is deposited on a cleaned quartz substrate (1×2 cm^2) at a substrate temperature of 50 ^oC by reactive magnetron sputtering. The details were mentioned elsewhere.[41] Then, a 60-nm a-Si film is deposited on a YSZ/quartz substrate by e-beam evaporation method at 300 ^oC. For comparison, an a-Si film is also deposited directly on a quartz without YSZ layer. Next, micro-crystallization of the a-Si films is carried out in N_2 ambient by a Q-switched Nd:YAG pulse laser (λ = 532 nm) with a repetition frequency of 10 Hz and a pulse duration of 6~7 ns. The laser irradiation energy density E is less than 120 mJ/cm^2 for reduction of surface roughness due to partial melting and unstable enlargement of grain size. The new two-step method is illustrated in Fig. 1(b), in comparison with the conventional one, where the poly-Si film thickness from the interface and the a-Si film thickness are denoted by d_p and d_a, respectively, and the total thickness of the Si film (d_p + d_a) is constant of 60 nm. For

the two-step method, the total pulse number N is kept constant of 16 or 100 while pulse numbers of initial stage N_i and growth stage N_g are 10~90 and 6~90, respectively, so as to keep $N = N_i + N_g$. The initial and growth energy densities ranges are 14–34 mJ/cm^2 and 70–117 mJ/cm^2, respectively.

The crystallization degree of Si films is estimated by two kinds of Raman spectroscopies. The first one is He-Ne system with the excitation wavelength of 633 nm. The absorption depth D for a-Si is more than 200 nm. So, the He-Ne system is used to evaluate average crystalline quality of a whole Si film. The second one is He-Cd system with the wavelength of 442 nm. Ds for a-Si and poly-Si are 20–30 nm and more than 200 nm, respectively. Therefore, the He-Cd system is used to evaluate the crystalline quality locally at the surface and interface of the Si film. The crystalline fraction X_c is determined by $X_c = (I_c + I_m)/(I_c + I_m + I_a)$ where I_c, I_m, and I_a are integrated intensities of crystalline silicon (c-Si), intermediate-crystalline silicon (m-Si), and a-Si peaks, respectively.[39,42] The grain size of poly-Si films after Secco-etching is observed by SEM.

3. Results and discussion

3.1. Si nucleation location and saturation behavior of X_c

At first, the Si nucleation observation result is mentioned in the conventional method. Figure 2 shows the He-Cd Raman spectra from the front and back side measurements of the Si/YSZ/glass at the energy density E and pulse number N of 78–80 mJ/cm^2 and 10, respectively. It can be seen that, from the front side measurement of Fig. 2(a), a very small c-Si peak might be observed. On the other hand, from the back side measurement of Fig. 2(b), a relative high and sharp c-Si peak clearly appears. This indicates that, at this energy

density, the crystallization growth is enhanced from the interface between the Si film and the YSZ layer, but little nucleation occurs near the surface of Si film. This enhancement of crystallization from the interface is considered to be owing to not only heterostructure (e.g. Si/SiO_2) but also the CI effect of YSZ layer.[39,43,44] If E is much higher than that of Fig. 2, the crystallization would be nearly completed, which shows no significant difference in crystallization behavior at the surface and interface of the Si film. On the other hand, if E is much lower, the nucleation and crystallization growth would be very few and local, which is hardly observed precisely by the He-Cd Raman spectroscopy.

Next, the saturation behavior of X_c is explained. The dotted line in Fig. 3 shows the theoretical calculation for the relation between the whole film absorptivity A and the poly-Si film thickness d_p as shown in Fig. 1(b). The absorptivity is defined as a ratio of $(E - E_R - E_T)/E$, where E_R is a reflected beam energy density at the Si film surface and E_T is a transmitted one at the YSZ layer interface. Also, in this figure, the experimental data for the relationship between the saturation X_c and irradiation energy density E are shown by the closed circles and the solid line as an eye guide. These two relations (i.e. $d_p - A$ and $X_c - E$) are shown together because they are interdependent each other, which is discussed later. For the calculation of the whole film absorptivity A, it is assumed that a coherent laser beam with $\lambda = 532$ nm is incident on the sample surface at normal angle and that the Si film is crystallized uniformly from the YSZ layer interface and the crystallization front progresses in parallel to the interface. Also, we consider multireflection in the sample consisting of Si film, YSZ layer, and glass substrate.[45,46] The refractive indices of the a-Si, poly-Si, YSZ, and the glass substrate at a wavelength of 532 nm are $n_{a\text{-}Si} \approx 4.53\text{-}i0.897$, $n_{poly\text{-}Si} \approx 4.15\text{-}i0.0428$, $n_{YSZ} \approx 2.18$, and $n_{SiO_2} \approx 1.46$, respectively.[47,48] The detailed derivation of A is

mentioned in the Appendix. It can be seen from Fig. 3 that A decreases with increasing d_p. Because the absorptivity of a-Si (~0.445) is much larger than that of poly-Si (~0.042) for the incident beam, increasing d_p leads to decrease d_a so that A should decrease in the case of a constant total Si film thickness of 60 nm. Also, in Fig. 3, increasing the irradiation energy density E brings increasing of the experimental saturation X_c, which is exactly counter to the relationship between A and d_p.

From the above results, we can explain the saturation X_c behavior to E as follows: At first, it can be postulated that the ratio between the poly-Si film thickness and the total thickness, $[d_p/(d_p+d_a)] = d_p$ (nm)/60, corresponds or roughly equals to the saturation X_c. That is, X_c (%) $= 100 \times d_p$ (nm)/60 $= 5d_p$ (nm)/3. This is possible because X_c shows the ratio between the crystallized volume and the total volume of the Si film, which are proportional to their thickness ratio. The amount of heat H generated due to optical absorption in the irradiated Si film can be proportional to a product $A \cdot E$ of absorptivity A and irradiation energy density E ($H \propto A \cdot E$), and the heat rises film temperature T_f ($T_f \propto H$). Therefore, T_f strongly depends on $A \cdot E$ ($T_f \propto A \cdot E$). Strictly speaking, temperature distribution in the film is not uniform and depends on the film depth position because the beam energy is decreased with the traveling or penetrating depth position in the film due to optical absorption. However, since the thermal diffusion length of a-Si and c-Si are calculated to be ~75 nm and ~738 nm at 300 K, respectively, for the pulse duration time of 6 ns, which are longer than the total film thickness of 60 nm. The film temperature T_f may become almost uniform at least after the pulse duration time. That is, $A \cdot E$ (mJ/cm^2) is dissipation energy in the film per unit area and heat H generated due to $A \cdot E$ is diffused instantaneously and uniformly in the Si film. Therefore, we can hypothesize that T_f is uniform in the film. At a very low E, the

crystallization cannot start because T_f is smaller than the critical crystallization temperature T_c. In order to induce and progress crystallization growth, T_f should be more than or equal to T_c. To keep T_f constant over T_c, the sample should be irradiated at a larger E. At the condition of $T_f \geq T_c$ and E = constant, the crystallization progresses continuously with increasing pulse number N. So, the thickness d_p of poly-Si film also increases, accompanied with the decrease of A as shown in Fig. 3. As a result, H and T_f are decreased because $H \propto A \cdot E$ and $T_f \propto H$. The crystallization is suspended or stopped and the crystalline fraction X_c becomes saturate when T_f decreases under T_c. In order to increase and keep T_f constant over T_c again, a larger E is needed at a smaller A because $T_f \propto A \cdot E$. Due to this negative feedback phenomenon, the X_c finally saturates under the condition of a fixed E. Owing to self-limiting process of the saturation behavior, crystallization of Si films can be performed in a relatively stable manner even if E is fluctuated within some range during irradiation.

3.2. Two-step method

Taking advantages of not only interface nucleation enhancement with suppression of bulk nucleation at lower E but also the energy-self-limiting crystallization, we have proposed the two-step method of Fig. 1(b). Without energy-self-limiting crystallization, stable process in the two-step method could be never expected. Figure 4 shows the He-Cd Raman spectra from the front and back side measurements of the Si/YSZ/glass crystallized by the two-step method. This sample, at first, was irradiated at the low initial energy density E_i of 18–22 mJ/cm^2 with the initial pulse number N_i of 10, followed by irradiation at the high growth energy density E_g of 78–80 mJ/cm^2 with the growth pulse number N_g of 6. The E_g is chosen in order to compare with the result of the conventional method in Fig. 2. From the front side

measurement of Fig. 4(a), no or a faint small c-Si peak might be observed like the conventional method of Fig. 2(a), which indicates that the near-surface crystallization hardly occurs. However, from the back side measurement, a higher and sharper c-Si peak is clearly observed, compared with the conventional one of Fig. 2(b). This means that the interface growth is more enhanced by the two-step method even with the smaller pulse number at the high energy density E_g and lower total irradiation energy density E_t, where $E_t = E \cdot N$ for the conventional and $E_t = E_i \cdot N_i + E_g \cdot N_g$ for the two-step. From this result, it can be considered that, in the two-step method, the initial irradiation at the low E_i induces nuclei on the YSZ interface with suppression of bulk nucleation, and that the irradiation at the high E_g then accelerates crystallization growth from the interface nuclei with a higher rate than in the conventional method.

Next, irradiation conditions of the initial stage, i.e., N_i and E_i are investigated and optimized. This is because these conditions are very important in the two-step method. If there is too few nucleation in the initial stage at a too low E_i, the crystallinity of Si film is not improved, compared with the conventional method due to the nearly same irradiation conditions. On the other hand, if, at a too high E_i, the nucleation not only occurs at the YSZ interface, but also in the bulk or near the surface of the Si film, the crystallization growth from bulk nuclei prevents the growth from interface nuclei. As a result, crystallinity of the Si film degrades. Figure 5(a) shows the dependences of FWHM of c-Si peak and crystalline fraction X_c on the pulse number $N_i = N\text{-}N_g$ ($N = 100$) for the Si/YSZ/glass case in the two-step method ($N_i \neq 0$), compared with the conventional one ($N_i = 0$). The closed squares and the opened circles indicate the data of X_c and FWHM of c-Si peak, respectively. Also, the energy densities for the initial and growth stages are 26–29 and 92–96 mJ/cm^2, respectively.

It can be seen that, at $N_i = 10$, the FWHM is reduced abruptly and the X_c increases from $N_i = 0$. Then, both FWHM and X_c decrease slightly with further increasing N_i. The decrease of X_c is due to the reduction of the irradiation number N_g or annealing time of high energy density E_g with increasing N_i. The slight decrease of FHWM with increasing N_i indicates that longer annealing time at a low energy density might promote interface nucleation, which has an effective force for direction alignment of the crystallization growth caused by irradiation with a high energy density E_g. From this figure, it can be concluded that the two-step method can improve crystalline quality of the Si film significantly. Under the condition of constant $N = 100$, we choose the conditions of $N_i = 10$ and $N_g = 90$ for the next investigation because the X_c is apparently maximum and the FWHM is relatively low.

We also investigated the dependences of crystallization degree in the crystallized Si films on the initial energy density E_i. This is because E_i is a very important factor to control location of nuclei generation, i.e., only on the YSZ interface or not. Figure 5(b) shows the dependences of FWHM and position k_p of c-Si peak, and crystalline fraction X_c on the initial E_i for the Si/YSZ/glass structure in the two-step method, where E_g, N_i, and N_g are fixed at 106–109 mJ/cm^2, 10, and 90, respectively. The growth energy density E_g is near but less than the critical melting energy density of Si film so that the Si film would not be intentionally melting-crystallized. On a whole, because of using a higher E_g than Fig. 5(a), the crystallized Si films show higher crystalline fraction or higher X_c and higher crystalline quality or lower FWHM.

It can be seen from Fig. 5(b) that the X_c increases with E_i to ~ 22 mJ/cm^2, then decreases with E_i in the higher range. The opposite tendency is observed for the FWHM. At E_i = 18.5–22 mJ/cm^2, the X_c is maximum while the FWHM is minimum. It is considered that, at

the E_i < 18.5 mJ/cm^2, a very small amount of nuclei might be generated at the interface between the Si film and the YSZ layer. Being irradiated at the high E_g, the crystallization growth from these interface nuclei proceeds quickly. Also, in the other interface region, new nuclei are formed and then crystallization proceeds quickly from there. However, the crystallization front may be not uniformly flat, or not parallel to the interface. That is, it may be rugged and irregular one. This irregular crystallization front might enhance random nucleation near the front and induce change of the growth direction. As a result, many small grains are formed after the crystallization at the high E_g. The X_c, therefore, is not so high and the FWHM is large at the E_i < 18.5 mJ/cm^2. At the higher E_i around 20 mJ/cm^2, a larger amount of interface nuclei might occur without bulk nucleation. By irradiation at the high E_g, the crystallization growth from these nuclei proceeds smoothy and the front is relatively flat and parallel to the interface, compared with the lower E_i case. Therefore, the crystalline fraction X_c increases significantly and the defect density is reduced, which leads to the decrease of FWHM. When E_i > 22 mJ/cm^2, the nucleation might occur not only at the interface but also in the bulk of the Si film slightly. The crystallization growth from bulk nuclei in the high E_g irradiation prevents the growth from interface nuclei partially. As a result, the X_c of the Si film decreases a little while the FWHM slightly increases. Also, it can be seen in Fig. 5(b), the peak positions are nearly the same for all values of initial energy density E_i and in the range from 515 to 517 cm^{-1}, which is lower than the peak position of single-crystalline Si (520 cm^{-1}). This indicates that the Si films exhibit tensile stress on the YSZ layer at all values of E_i. In our samples, the film stress is due to the densification during phase transition from amorphous to crystalline.[39)] So, it is considered that the variation of FWHM with E_i for the Si/YSZ/glass is not so related with the film

stress. From the above discussion, the value E_i = 18.5–22 mJ/cm^2 can be determined to be nearly optimum from the viewpoints of Si film crystalline fraction and crystallinity.

Figures 6(a) and 6(b) show the He-Ne Raman spectra of the Si/glass and Si/YSZ/glass structures by the two-step method. In Fig. 6(a), the both structures are irradiated under the condition (A) of E_i = 18–22 mJ/cm^2 and E_g = 106–109 mJ/cm^2, which is the optimized condition for Si/glass structure. Figure 6(b) shows the spectra of only Si/YSZ/glass structure under its optimized condition of E_i = 20–24 mJ/cm^2 and E_g = 111–114 mJ/cm^2, which is labelled as condition (B). It can be seen from Fig. 6(a) that the shoulder of amorphous phase (denoted by the dash circle) in the spectrum of the Si/glass is smaller, indicating the higher X_c, than in the Si/YSZ/glass. Moreover, the height and width of crystalline Si peaks are the same for the both structures, indicating the same FWHMs. On the other hand, under the optimized condition (B) for the Si/YSZ/glass as shown in Fig. 6(b), obviously higher crystalline peak intensity with much smaller a-Si phase shoulder can be observed, compared with those in Fig. 6(a). Therefore, the higher X_c and smaller FWHM can be obtained.

Table I shows the comparison of the typical values of X_c and FWHM of c-Si peak of the Si/glass and the Si/YSZ/glass for the conventional method with N = 100 and the two-step method with N_i = 10 and N_g = 90, which are obtained from the He-Ne Raman spectra analysis. For the conventional method, the samples were irradiated at a constant E = 104–106 mJ/cm^2. The obtained crystallinities (crystalline fraction X_c and FWHM) of Si/glass and Si/YSZ/glass structures by the conventional method are labelled as ① and ②, respectively, in Table I. In the two-step method, the two kinds of irradiation conditions were used, which are condition (A) and condition (B) as the same with those mentioned in Fig. 6. The obtained X_c and FWHM of Si/glass and Si/YSZ/glass structures by the condition (A) are

labelled as ③ and ④, respectively, in Table I. The obtained crystallinity of Si/YSZ/glass structure by the condition (B) is labelled as ⑤ in Table I. The both optimized E_i and E_g for the Si/YSZ/glass are a little higher than those for the Si/glass. This is because the calculated absorptivity of the a-Si film in the a-Si/glass structure (~0.546) is higher than that in the a-Si/YSZ/glass structure (~0.445). A similar calculation result is obtained in the case of a poly-Si film, but the absorptivities of the poly-Si films are much smaller values, i.e., ~0.075 and ~0.042 for the poly-Si/glass and the poly-Si/YSZ/glass structures, respectively.[39] This means that, at the same irradiation condition, Si film in the Si/glass is heated more than that in the Si/YSZ/glass. This suggests us that, in order to compare these two structures fairly, we should estimate Si films crystallized at their own optimized conditions. This will be done and discussed in detail later. At first, it can be clearly seen that, the crystalline quality of crystallized Si films is more improved by the two-step method (③ and ④) for both the Si/glass and Si/YSZ/glass structures, compared with the conventional method (① and ②). That is, the higher X_c and the smaller FWHM are obtained by the two-step method in spite of using the same total pulse number and the lower total irradiation energy density E_t. The reason for improvement in crystallinities of the Si film on, for example, YSZ/glass by the two-step method is discussed later using a growth model. Next, we compare the Si/YSZ/glass case ④ with the Si/glass case ③ in the two-step method. Although X_c = 82% of the Si/YSZ/glass is apparently smaller than 87% of the Si/glass, whose difference is over the estimation error of ± 2%, FWHM of the former is nearly equal to 6.0 of the latter within the estimation error of ±0.5. This indicates that there is still a room to get larger X_c and better crystalline quality for the Si/YSZ/glass structure by optimizing E. Actually, using the optimized irradiation condition for the Si/YSZ/glass structure in the two-step method, we

obtain the higher X_c and smaller FWHM in ⑤ than in ③ and ④. From these results, it can be concluded that the better crystalline quality of the Si film can be obtained on the YSZ/glass than on the glass substrate for both the conventional and two-step methods, which may be due to the CI effect of the YSZ layer.

In order to show up the effect of the two-step method clearly, using SEM, we observed Secco-etched Si films crystallized by the both conventional and two-step methods. The images are shown in Fig. 7 and the irradiation conditions are the same as Table I. Figure 7(a) shows the SEM image of the Si film irradiated by the conventional method while Figs. 7(b), (c), and (d) show those by the two-step method, where the sample structures are Si/YSZ/glass except for (b), i.e., Si/glass. The labels ②, ③, ④, and ⑤ in Fig. 7 correspond to the number or the same irradiation conditions in Table I.

Firstly, from the comparison between Fig. 7(a) for the conventional and Fig. 7(c) for the two-step, it can be seen that larger-size grains are obtained in the Si/YSZ/glass structure by the two-step method. This clearly indicates the effectiveness of the two-step method in crystallization promotion of a-Si film. Next, we compare the Si film on glass and on YSZ in the two-step method at the same irradiation condition as shown in Figs. 7(b) and 7(c), respectively. It can be found easily that difference in grain size or non-uniform grain size is larger in the Si/glass than in the Si/YSZ/glass, for instance, as shown by circles in Figs. 7(b) and 7(c). When the Si/YSZ/glass is irradiated at its optimized condition as shown in Fig. 7(d), the grain size apparently becomes larger than the one for the Si/glass at the optimized irradiation condition [Fig. 7(b)]. This can be explained as follows: In the initial stage at the low energy density E_i and the small pulse number N_i for each structure, the Si nucleation only occurs on the interface between the Si film and the underlayer (SiO_2 or YSZ) for the

both structures. However, in the Si/glass, random Si nucleation occurs on the interface due to the lack of crystallographic information of glass substrate. On the other hand, in the Si/YSZ/glass, thanks to the CI effect of YSZ layer, the uniform nucleation may occur at the YSZ interface. With higher energy density E_g and larger pulse number N_g in the growth stage, for the Si/glass structure, direction and rate of the crystallization growth from the individual nucleus are not uniform due to the random nucleation. Also, since the non-uniform crystallization growth prevents smooth crystallization process, bulk nucleation might occur before crystallization completion. On the other hand, for the Si/YSZ/glass structure, crystallization proceeds from the interface more smoothy due to interface nuclei induced promptly by YSZ. Therefore, grains in the Si/YSZ/glass have larger and more uniform size than those in the Si/glass.

Carefully seeing Fig. 7(d), some twins can be observed as straight lines along the Si film surface, some of which are indicated by the arrows inside. It is reported that a typical deformation twinning mode in diamond-type crystals is {111}/⟨112⟩, which is the major defects mode observed in a stressed crystal.[49] It is assumed that the twins appeared in Fig. 7(d) is due to {111}/⟨112⟩ mode, the surface orientation of the Si film might be (110).

Based on the aforementioned experimental results and discussion, we discuss a growth model of the Si film crystallization on the YSZ layer for the conventional and the two-step methods as shown in Fig. 8. In the conventional method at a high energy density E [Fig. 8(a)], although crystallization from the interface nuclei is more preferable than in the bulk of Si film thanks to the YSZ layer, crystallization growth from the interface is impeded by the bulk random nucleation and growth. This might be due to the high nucleus density at a high E and the lack of crystallographic information in bulk of the a-Si film.[39] On the other hand,

in the two-step method of Fig. 8(b), nucleation preferably occurs in the a-Si film just on the YSZ layer with suppression of bulk nucleation in the initial stage of a low E_i. Then, in the growth stage of a high E_g, crystallization from the interface nuclei proceeds in a cone-shape at a high rate toward the surface. Therefore, the crystallized Si film by the two-step method has higher X_c and much smaller FWHM as well as larger grain size than those of the conventional one as shown in Table I and Fig. 7.

4. Conclusion

We successfully crystallized a-Si films on YSZ CI layers by the new two-step method of PLA without intentionally melting. Their film properties were investigated and compared with those of the conventional one by Raman spectroscopies and SEM. The results of the conventional method showed that, for the Si/YSZ/glass structure, the nucleation occurs faster on the YSZ interface than in the bulk of a-Si film at the low energy density E. Moreover, the saturation behavior of crystalline fraction X_c at the high E was found to be a self-limiting process. Based on these two results, we proposed the two-step method for further improving crystallinity of the Si films and obtained the following results: The crystallization growth from the YSZ interface is more enhanced by the two-step method than by the conventional one. The Raman analysis and SEM observation show that the higher X_c, smaller FWHM, and larger grain size were obtained by the two-step method compared with the conventional one at the same total pulse number N and higher total irradiation energy density E_t. Comparing the two structures of Si/YSZ/glass and Si/glass at their own optimized irradiation conditions, we obtained the higher X_c and smaller FWHM in the former. From these results, it can be concluded that the crystalline quality of Si films is much improved by using the two-step method with the YSZ CI layer in PLA.

Acknowledgment

This work was partially supported by Marubun Research Promotion Foundation.

Appendix

In this section, we present the detailed calculation of the whole Si film absorptivity *A*, which is mentioned in Fig. 3. The assumptions for this calculation are mentioned in the section of results and discussion. Figure (A·1) shows the schematic calculation model of the sample structure in accordance with the actual experimental conditions. Here, we also assume that the reflected beam from the bottom of glass substrate is neglected. This is because the reflected power from the bottom of the substrate is very small (less than 5% for incident angle ≤ 20°) and the thickness of glass is ~0.5 mm which is more than 900 times the wavelength λ = 532 nm. The reflection coefficient r_j and transmission coefficient t_j at the *j-1*/ *j* interface from layer *j-1* to layer *j* and from layer *j* to layer *j-1*, respectively, in the case of normal incidence are given by

$$r_j = \frac{n_j - n_{j-1}}{n_j + n_{j-1}} \text{ and } t_j = \frac{2n_j}{n_j + n_{j-1}}, \quad j = 1, 2, 3 \tag{A·1}$$

where n_j and n_{j-1} are refractive indies of layers *j* and *j-1*, respectively. The reflection and transmission coefficients R_j and T_j, respectively, at each interface in the sample structure of Fig. (A·1), taking account of multireflection in the underlayers, are calculated by

$$R_j = \frac{r_{j+1} + R_{j-1}\, exp\left(-2i\phi_j\right)}{1 + r_{j+1} R_{j-1}\, exp\left(-2i\phi_j\right)} \text{ and } T_j = \frac{t_{j+1} + T_{j-1}\, exp\left(-i\phi_j\right)}{1 + r_{j+1} R_{j-1}\, exp\left(-2i\phi_j\right)}, \quad j = 1, 2, 3 \tag{A·2}$$

where $R_o = r_1$, $T_o = t_1$, and $\phi_j = 2\pi \times n_j \times d_j/\lambda$, in which d_j is the thickness of layer *j*. It is noted that if the layer *j* is absorbing, its refractive index contains two parts of real and

imaginary. This means that n becomes $\tilde{n} = n - ik$. The power reflectivity $\mathcal{R}$ and power transmissivity $\mathcal{T}$, taking account of all multireflections, are given by:

$$\mathcal{R} = |R_3|^2 = R_3 \times R_3^* \quad \text{and} \quad \mathcal{T} = \frac{n_o}{n_4}|T_3|^2 = \frac{n_o}{n_4} \times T_3 \times T_3^*, \tag{A·3}$$

in which R_3^* and T_3^* are the conjugates of R_3 and T_3, respectively. The whole Si film absorptivity A, which is defined as the fraction of dissipated power of the laser beam when it goes through the Si film, is determined by:

$$A = 1 - \mathcal{R} - \mathcal{T}. \tag{A·4}$$

References

1) P. F. Carcia, R. S. McLean, M. H. Reilly, and G. Nunes, Jr., Appl. Phys. Lett. **82**, 1117 (2003).

2) K. Nomura, H. Ohta, K. Ueda, T. Kamiya, M. Hirano, and H. Hosono, Science **300**, 1269 (2003).

3) K. Nomura, H. Ohta, A. Takagi, T. Kamiya, M. Hirano, and H. Hosono, Nature **432**, 488 (2004).

4) C. D. Dimitrakopoulos and P. R. L. Malenfant, Adv. Mater. **14**, 99 (2002).

5) H. Y. Choi, S. H. Kim, and J. Jang, Adv. Mater. **16**, 732 (2004).

6) P. G. LeComber, W. E. Spear, and A. Ghaith, Electron. Lett. **15**, 179 (1979).

7) T. Sameshima, S. Usui, and M. Sekiya, IEEE Electron Device Lett. **7**, 276 (1986).

8) A. Suresh and J. F. Muth, Appl. Phys. Lett. **92**, 033502 (2008).

9) J. K. Jeong, H. W. Yang, J. H. Jeong, Y. -G. Mo, and H. D. Kim, Appl. Phys. Lett. **93**, 123508 (2008).

10) K. Nomura, T. Kamiya, M. Hirano, and H. Hosono, Appl. Phys. Lett. **95**, 013502 (2009).

11) R. S. Potember, T. O. Poehler, and D. O. Cowan, Appl. Phys. Lett. **34**, 405 (1979).

12) L. Ma, S. Pyo, J. Ouyang, Q. Xu, and Y. Yang, Appl. Phys. Lett. **82**, 1419 (2003).

13) M. J. Powell, IEEE Trans. Electron Devices **36**, 2753 (1989).

14) M. J. Powell, Appl. Phys. Lett. **43**, 597 (1983).

15) F. R. Libsch and J. Kanicki, Appl. Phys. Lett. **62**, 1286 (1993).

16) H. Matsumura, Jpn. J. Appl. Phys. **30**, L1522 (1991).

17) J. K. Holt, M. Swiatek, D. G. Goodwin, R. P. Muller, W. A. Goddard III, and H. A. Atwater, Thin Solid Films **395**, 29 (2001).

18) P. Reinig, F. Fenske, W. Fuhs, A. Schopke, and B. Selle, Appl. Surf. Sci. **210**, 301 (2003).

19) C. Ipri and G. Kaganowicz, IEEE Trans. Electron Devices **35**, 708 (1988).

20) G. Liu and S. J. Fonash, Appl. Phys. Lett. **55**, 660 (1989).

21) R. Kakkad, J. Smith, W. S. Lau, S. J. Fonash, and R. Kerns, J. Appl. Phys. **65**, 2069 (1989).

22) L. Haji, P. Joubert, J. Stoemenos, and N. A. Economou, J. Appl. Phys. **75**, 3944 (1994).

23) J. N. Lee, Y. W. Choi, B. J. Lee, and B. T. Ahn, J. Appl. Phys. **82**, 2918 (1997).

24) S. F. Gong, H. T. G. Hentzell, A. E. Robertsson, L. Hultman, S. E. Hörnström, and G. Radnoczi, J. Appl. Phys. **62**, 3726 (1987).

25) G. Radnoczi, A. Robertsson, H. T. G. Hentzell, S. F. Gong, and M. A. Hasan, J. Appl. Phys. **69**, 6394 (1991).

26) S. Y. Yoon, K. H. Kim, C. O. Kim, J. Y. Oh, and J. Jang, J. Appl. Phys. **82**, 5865 (1997).

27) Z. Jin, G. A. Bhat, M. Yeung, H. S. Kwok, and M. Wong, J. Appl. Phys. **84**, 194 (1998).

28) S.-W. Lee, Y.-C. Jeon, and S.-K. Joo, Appl. Phys. Lett. **66**, 1671 (1995).

29) S.-I. Jun, Y.-H. Yang, J.-B. Lee, and D.-K. Choi, Appl. Phys. Lett. **75**, 2235 (1999).

30) M. Wong, Z. Jin, G. A. Bhat, P. C. Wong, and H. S. Kwok, IEEE Trans. Electron Devices **47**, 1061 (2000).

31) C.-Y. Hou and Y. S. Wu, Jpn. J. Appl. Phys. **44**, 7327 (2005).

32) J. C. C. Fan and H. J. Zeiger, J. Appl. Phys. **27**, 224 (1975).

33) T. Sameshima, M. Hara, and S. Usui, Jpn. J. Appl. Phys. **28**, L2131 (1989).

34) S. Higashi, N. Ando, K. Kamisako, and T. Sameshima, Jpn. J. Appl. Phys. **40**, 731 (2001).

35) S.-G. Ryu, I. Gruber, C. P. Grigoropoulos, D. Poulikakos, and S.-J. Moon, Thin Solid Films **520**, 6724 (2012).

36) S. Horita and H. Sukreen, Appl. Phys. Express **2**, 041201 (2009).

37) S. Horita and S. Hana, Jpn. J. Appl. Phys. **49**, 105801 (2010).

38) M. T. K. Lien, K. Mochizuki, and S. Horita, Proc. of AM-FPD'13, 2013, p. 175.

39) M. T. K. Lien and S. Horita, Jpn. J. Appl. Phys. **53,** 03CB01 (2014).

40) M. T. K. Lien and S. Horita, Proc. of IDW'13, 2013, p. 655.

41) S. Hana, K. Nishioka, and S. Horita, Thin Solid Films **517**, 5830 (2009).

42) S. Ray, S. Mukhopadhyay, T. Jana, and R. Carius, J. Non-Cryst. Solids **299–302**, 761 (2002).

43) L. Haji, P. Joubert, M. Guendouz, N. Duhamel, and B. Loisel, MRS Proc. **230**, 177 (1992).

44) J. N. Lee, B. J. Lee, D. G. Moon, and B. T. Ahn, Jpn. J. Appl. Phys. **36**, 6862 (1997).

45) H. Kaki, T. Ootani, and S. Horita, MRS Proc. **808**, 283 (2004).

46) S. Horita, H. Kaki, and K. Nishioka, Jpn. J. Appl. Phys. **46,** 3527 (2007).

47) D. Edwards, in *Handbook of Optical Constants of Solids*, ed. E. Palik (Academic Press, New York, 1985) pp. 564, 578.

48) S. Heiroth, R. Ghisleni, T. Lippert, J. Michler, and A. Wokaun, Acta Mater. **59**, 2330 (2011).

49) Y. Komem and Z. A. Weinberg, J. Appl. Phys. **56**, 2213 (1984).

Figure captions

Fig. 1. (Color online) Schematic illustrations of crystallization in the Si/YSZ/glass for (a) the conventional and (b) the new two-step methods together with the irradiation conditions. d_p is thickness of the crystallized Si film from the YSZ interface and d_a is thickness of the remaining a-Si film.

Fig. 2. (Color online) He-Cd Raman spectra of the Si/YSZ/glass crystallized by the conventional method from (a) the front side and (b) the back side measurements. The dotted circles indicate regions of crystalline Si peak**.**

Fig. 3. (Color online) Theoretical calculation curve of the Si film absorptivity as a function of the poly-Si thickness d_p (dotted line) from the YSZ interface and experimental data relationship between saturation crystalline fraction X_c and pulse energy density E (closed circles and solid line) by the conventional method.

Fig. 4. (Color online) He-Cd Raman spectra of the Si/YSZ/glass crystallized by the two-step method from (a) the front side and (b) the back side measurements. The dotted circles indicate regions of crystalline Si peak**.**

Fig. 5. (Color online) Dependences of c-Si peak FWHM and crystalline fraction X_c on (a) the initial pulse number N_i for the two-step ($N_i \neq 0$) and conventional ($N_i = 0$) methods, and (b) dependences of FWHM and position k_p of c-Si peak, and X_c on the initial energy density E_i for the two-step method. The upper horizontal indicates the pulse number of growth stage $N_g = N- N_i$ with $N = 100$."

Fig. 6. (Color online) He-Ne Raman spectra of (a) Si/glass and Si/YSZ/glass under the condition (A) of E_i = 18–22 mJ/cm^2 and E_g = 106–109 mJ/cm^2 and (b)

Si/YSZ/glass under condition the (B) of E_i = 20–24 mJ/cm^2 and E_g = 111–114 mJ/cm^2. The shoulders of a-Si phase are circled insides.

Fig. 7. (Color online) SEM images of the Secco-etched crystallized Si films by the conventional and two-step methods. (a), (b), (c), and (d) irradiation conditions are the same with the labels of ②, ③, ④, and ⑤ of Table I, respectively. Notice that the difference in grain size uniformity between (b) and (c) is circled insides. Arrows in Fig. (d) indicate examples of twins on the film surface.

Fig. 8. (Color online) Si film crystallization growth models of Si/YSZ/glass for the (a) conventional and (b) two-step methods.

Fig. A·1. (Color online) Schematic model of the sample structure for the whole Si film absorptivity calculation.

Table

Table I Crystalline fraction X_c and FWHM of c-Si peak of Si/glass and Si/YSZ/glass for the conventional and two-step methods. The two-step method has the two kinds of irradiation conditions (A) and (B).

Method		Irradiation condition	Si/glass	Si/YSZ/glass
Conventional		E = 104 – 106 mJ/cm^2, N = 100	X_c = 79% ① FWHM = 8.1	X_c = 75% ② FWHM = 7.6
Two-step	**(A)**	E_i = 18 – 22 mJ/cm^2, N_i = 10 E_g = 106 – 109 mJ/cm^2, N_g = 90 (optimized for Si/glass)	X_c = 87% ③ FWHM = 6.0	X_c = 82% ④ FWHM = 6.1
	(B)	E_i = 20 – 24 mJ/cm^2, N_i = 10 E_g = 111 – 114 mJ/cm^2, N_g = 90 (optimized for Si/YSZ/glass)	/	X_c = 91% ⑤ FWHM = 5.2

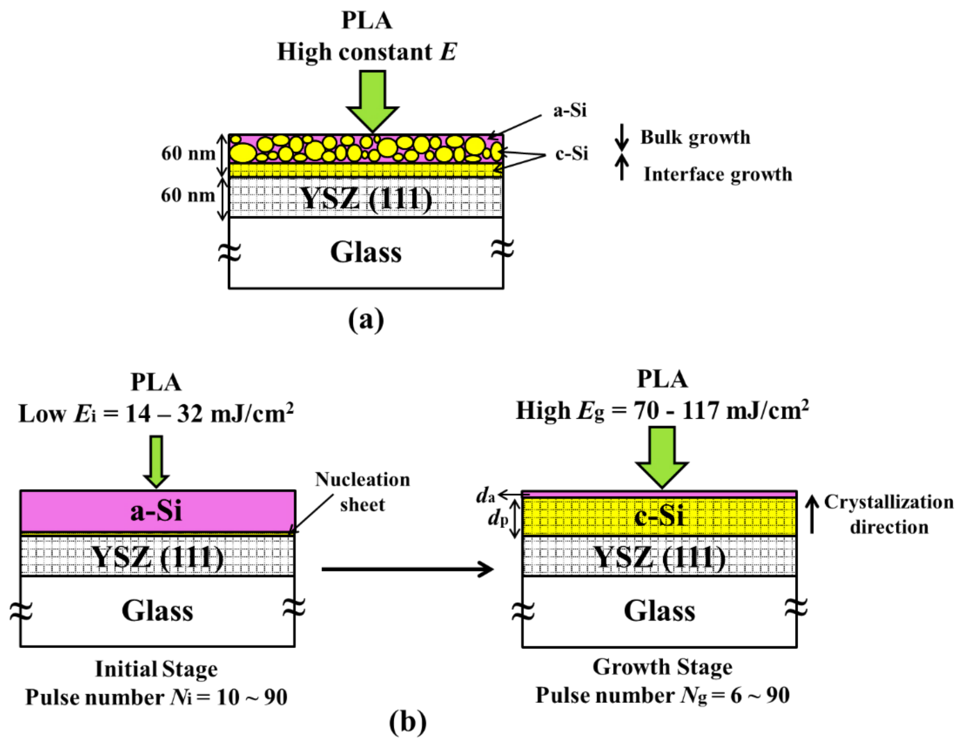

Fig. 1. Mai Thi Kieu Lien and Susumu Horita

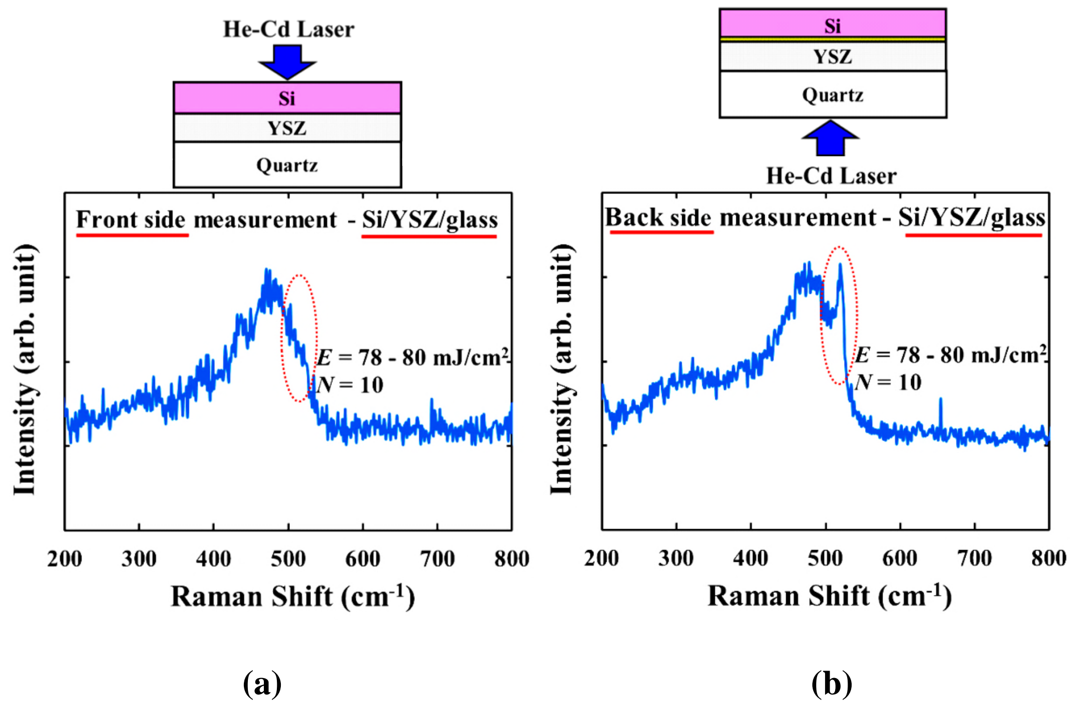

Fig. 2. Mai Thi Kieu Lien and Susumu Horita

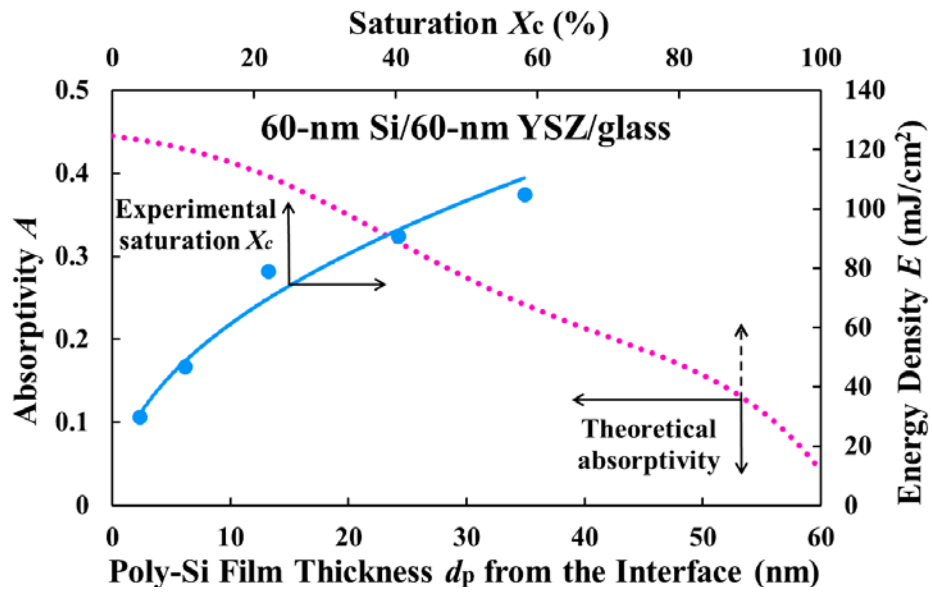

Fig. 3. Mai Thi Kieu Lien and Susumu Horita

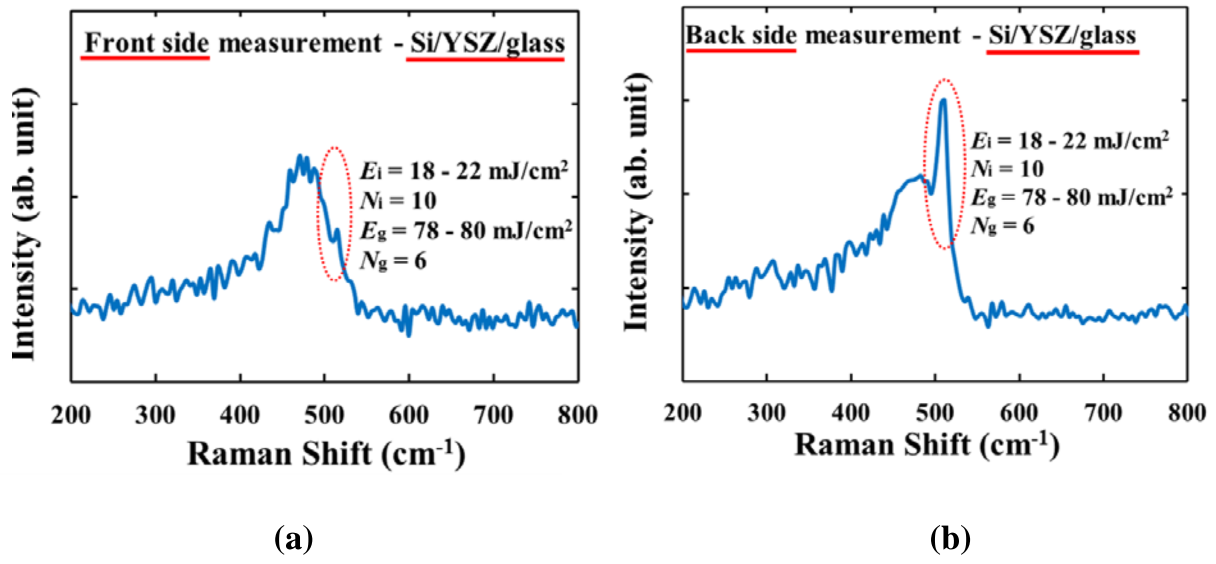

Fig. 4. Mai Thi Kieu Lien and Susumu Horita

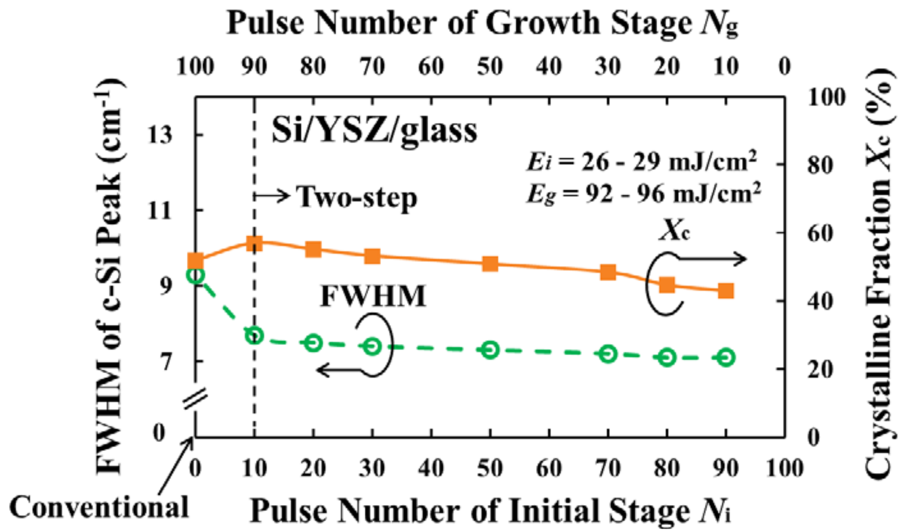

(a)

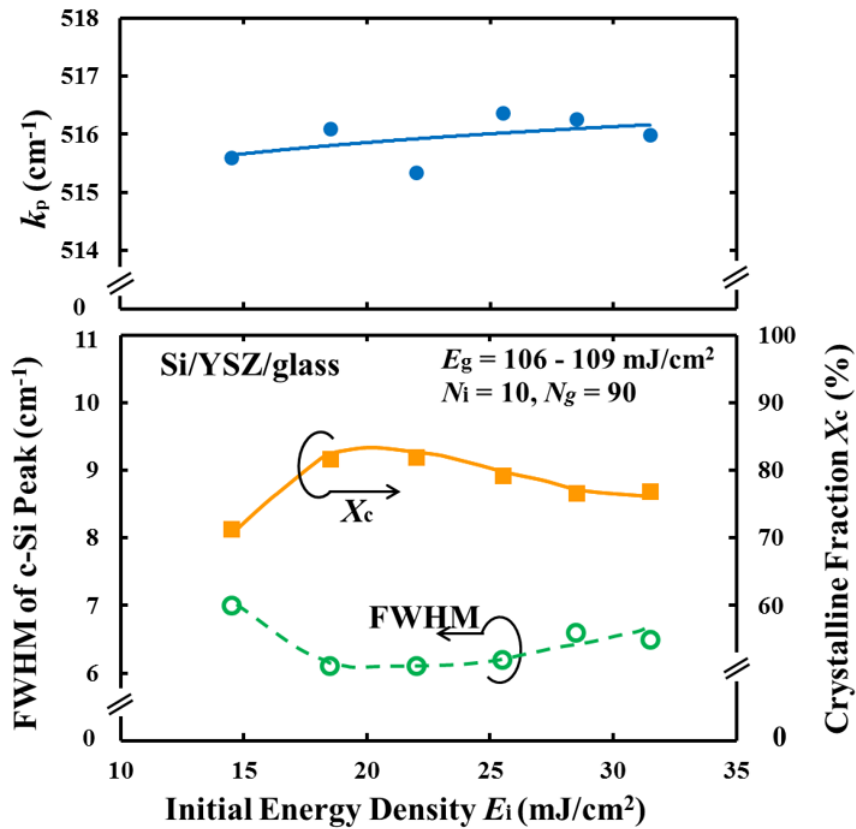

(b)

Fig. 5. Mai Thi Kieu Lien and Susumu Horita

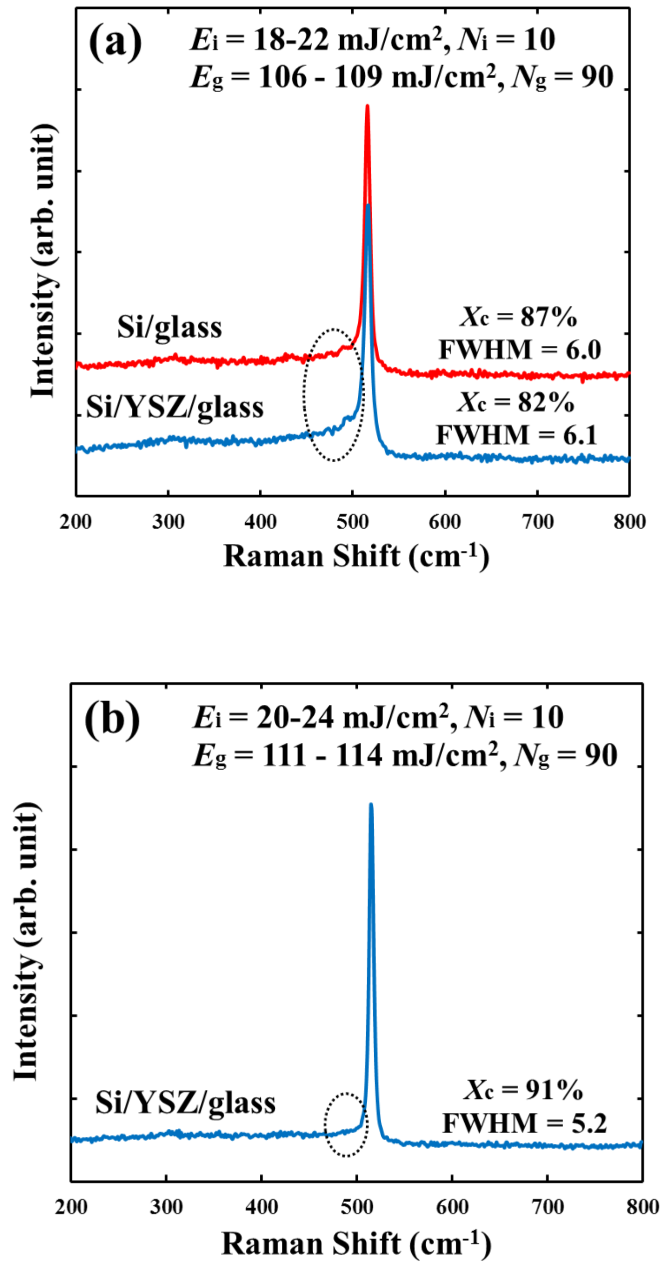

Fig. 6. Mai Thi Kieu Lien and Susumu Horita

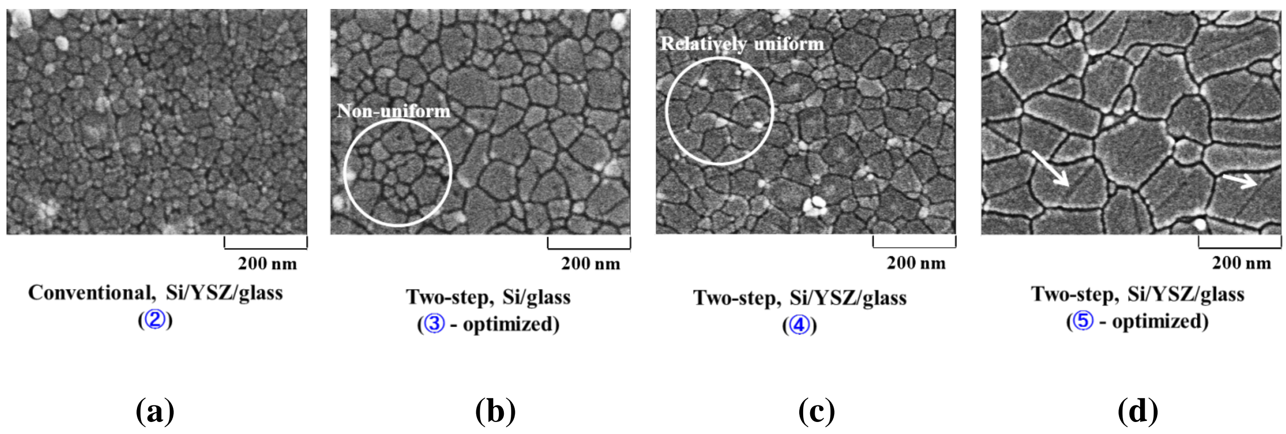

Fig. 7. Mai Thi Kieu Lien and Susumu Horita

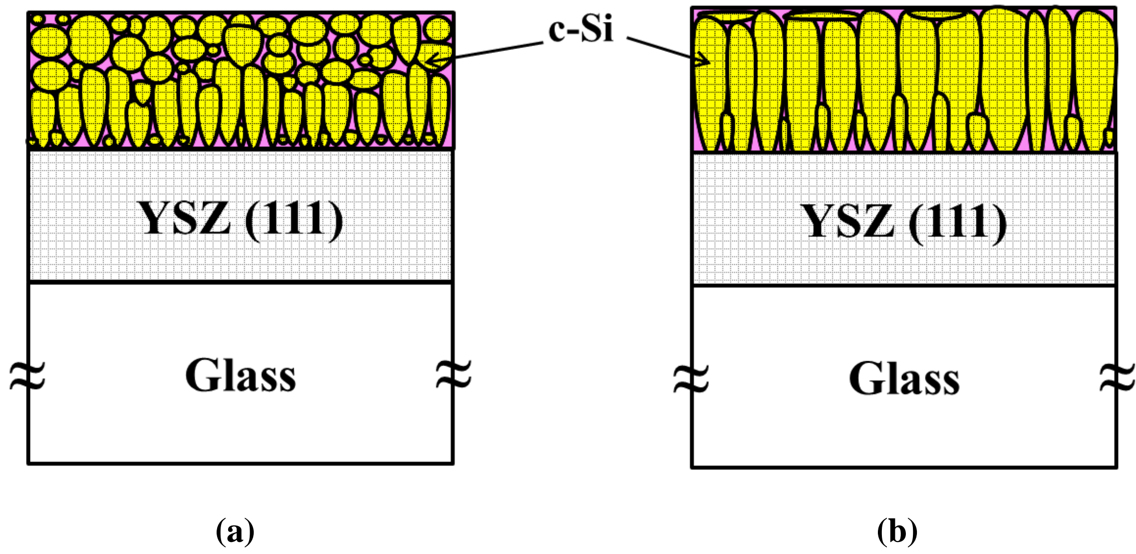

Fig. 8. Mai Thi Kieu Lien and Susumu Horita

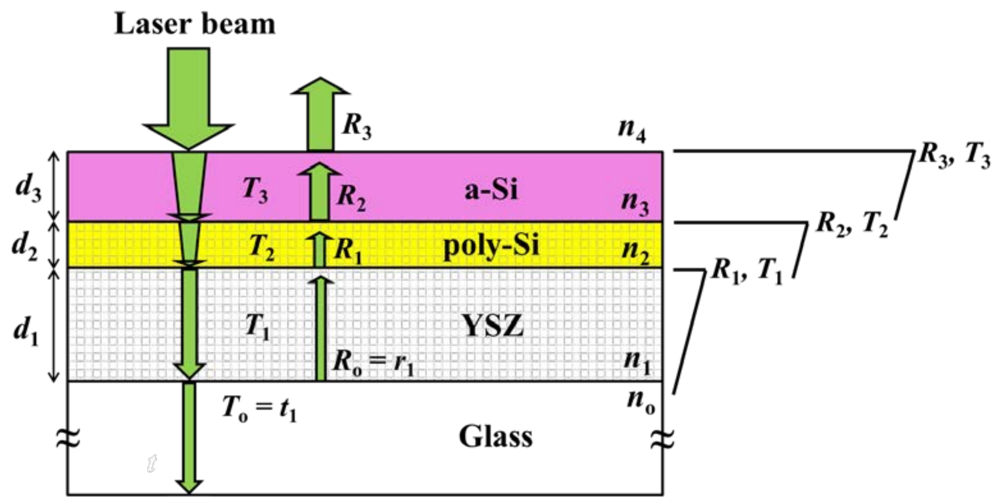

Fig. (A·1). Mai Thi Kieu Lien and Susumu Horita